INTERNATIONAL JOURNAL OF GEOMATICS AND GEOSCIENCES
Volume 4, No 4, 2014

Research article ISSN 0976 – 4380

Hydrothermal stress and damage risk in the stones of the castle of Chambord-France

Saad Al-Omari[1,2], Xavier Brunetaud[1], Kevin Beck[1], Muzahim Al-Mukhtar[1]
[1]CNRS-Centre de Recherche sur la Matière Divisée, 1 Rue de la Ferollerie, 45100 Orléans, France
[2]Department of Civil Engineering, College of Engineering, Mosul University, Al-Majmooah Street, Mosul, Iraq
muzahim.al-mukhtar@univ-orleans.fr

ABSTRACT

The aim of this paper is to assess the risk of climate-induced damage to stone through the calculation of hydrothermal stresses. The stone studied is tuffeau, the main building stone of the Castle of Chambord. The climate is assessed though measurement of the stone temperature and relative humidity using sensors inserted into the stones of the castle. The mechanical properties required for stress calculation are the elastic modulus, the Poisson's ratio and the hydrothermal strain. A numerical model based on restrained strain was used to estimate the hydrothermal stresses, which were analysed through the calculation of their daily variation, or alternatively by comparison with core behaviour. The parameters studied include the depth in the stone, the orientation of the walls, the alternative calculation methodology, and an optional correction of stone data due to sensor accuracy. Results show that the risk of damage to the stone exposed to climate fluctuations can be significant: joint cracking due to tension near the stone surface, and surface buckling due to compression for stones already subjected to spalling, leading to crack propagation. The risk decreases with depth, and is maximal on the south wall. Sensor accuracy for high relative humidity proved to be a significant issue.

Keywords: Damage risk assessment, hygrothermal stress, spalling, tuffeau, Castle of Chambord

1. Introduction

Sustainable conservation of the built heritage involves studying the stresses experienced by materials of the monument in question, as this can provide key information to reduce the progress of damage, and to choose appropriate solutions for restoration.

Cultural heritage buildings are made of stone that must withstand the stresses induced by the loads of the structure itself, and on a more local scale, the stresses induced by surface phenomena: salt or ice crystallization, and thermal and hygric dilation. These surface phenomena are induced by interaction between local climate conditions and the properties of the stones. The monitoring of field temperature and humidity data, added to an appropriate characterization of the stone properties, are therefore prerequisites for such work.

Recently, several studies have investigated the mechanism that leads to degradation of the stones in the Castle of Chambord. Some of these studies involved the multi-scale experimental physical, chemical, and mechanical characterization of stone behaviour, in addition to laboratory ageing tests (Al-Omari et al., 2013b; Janvier-Badosa et al., 2013, 2010). Others concerned the organization of all the data collected in a 3D documentation platform,

the so-called digital health record, to be used as a diagnostic tool and decision support in the conservation and restoration planning phase (Stefani et al., 2013).

Several previous studies explored the impact of climatic conditions on the decaying processes of stones (Al-Omari et al., 2013a; Bonazza et al., 2009a and b; Ponziani et al., 2012; Eklund, 2008; Camuffo, 1998; Camuffo and Sturaro, 2001; Moropoulou et al., 1995; Viles, 2005). The work presented in this study is part of a research program on the degradation mechanisms of building stones in the Castle of Chambord. The paper focuses on assessing the risk of damage to the stone at different depths due to variation in the local climatic conditions through calculation of the induced hygrothermal stress, building on two previous studies (Al-Omari et al., 2013a, 2014). The first one aimed at assessing different damage processes such as thermal stress, condensation, and freezing-thawing cycles that could lead to degradation of the stone. The second one involved the coupled hygrothermal characterization of the stone elastic properties (i.e. elastic modulus, Poisson's ratio and hygrothermal strain). The present paper focuses on the calculation of stresses from restrained dilations. While previous attempts of stress calculation were limited to the effect of restrained thermal dilation (σ_T), with standard material characterization, the present one treats the coupled hygrothermal stress ($\sigma_{T\text{-}H}$) based on the coupled hygrothermal characterization of stone elastic properties. Moreover, the main application of this paper is not limited to the calculation of compressive stresses, but also covers tensile stresses, which may be more critical as the tensile strength of stone is weaker than the compressive strength.

2. Site, methods, climate data, and material characterisation

2.1 Site, the Castle of Chambord

The Castle of Chambord, Figure (1) is one of the most famous castles in the world as it is an emblem of French Renaissance architecture. It blends traditional French medieval forms with classical Renaissance structures. Its construction began in 1519, and reached completion in 1547, then changed little until 1639, when Louis XIV restored and furnished the castle. Further restorations took place at different periods in the 20th century. The Castle of Chambord has been part of the UNESCO World Heritage list since 1981.

This study focuses on the stones located in the walls of the east tower of the Castle, for three main reasons, Figure (1). Firstly, most of the stones in the walls of the east tower are original (not restored). Secondly, the east tower includes many highly degraded stones, with two main patterns of degradation: biological colonization (different types of lichens and mosses) and stone detachment in the form of stone spalling and exfoliation (Janvier-Badosa et al., 2013). Lastly, the semi-circular shape of the east tower makes it possible to study two different wall orientations, north- and south-facing, and thus to assess the effect of the wall orientation on the spatial distribution of the hygrothermal stresses induced within the stone.

2.2 Local climatic conditions

The Castle of Chambord is located in a rural area about 150 km to the south-west of Paris, approximately 84 m above average sea level. The area surrounding the castle is subjected to a mild humid temperate climate with moderately warm summers and no dry season. The meteorological data recorded during 1997-2012 at Bricy Air-Base station, about 45 km NE of the castle of Chambord, Figure (1), revealed that the average annual temperature is 11.4 °C, while daily variations are often in excess of 20 °C and 70% for stone temperature and stone humidity, respectively (Al-Omari et al., 2013a).

The digital thermal-humidity sensors FHAD-46x were used to measure the stone temperature (accuracy 1.3% for a temperature range from -20°C to 80°C) and stone humidity (accuracy 1.8% for humidity between 0%-90%). These sensors were installed on the stone surface and inserted at different depths (15, 30, 50 and 250 mm) inside the stones on both the north and south walls. The measurements of stone data lasted three years, from June 2009 to May 2012. The readings were recorded every 30 minutes, giving a total of 52560 values for temperature and humidity for each case studied (at different depths within the stone and at two different orientations).

An example of stone data is presented in Figure (2). It shows the daily maximum and minimum values of temperature and relative humidity, at 15 and 250 mm depth inside the stones located on the south wall, during one year. The recorded data revealed that the highest temperature and humidity variations occur at a depth of 15 mm inside the stone. At this depth, the daily difference between the extreme values of temperature and humidity can exceed 20°C and 30%, respectively, whereas at a depth of 250 mm, low or negligible variations were observed for both temperature and humidity (i.e. below 3°C for temperature and below 0.5% for humidity).

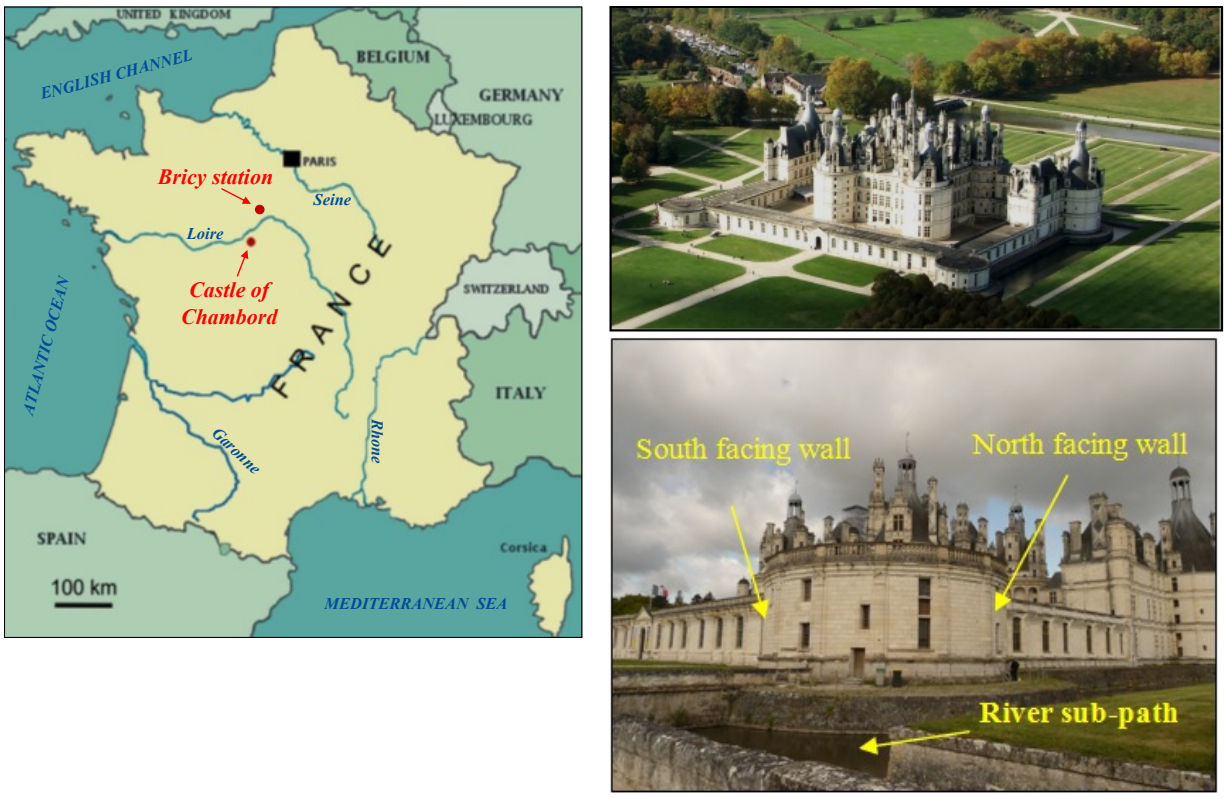

Figure 1: Geographical setting of the Castle of Chambord (*left*); the Castle of Chambord-aerial view "copyright: Domaine national de Chambord" (top right); the east tower of the castle (bottom right)

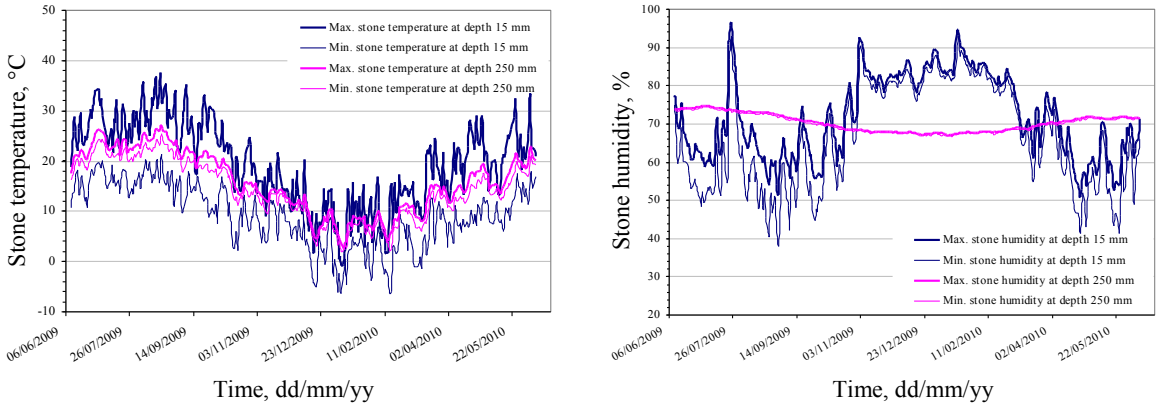

Figure 2: Daily maximum and minimum values of temperature (left) and relative humidity (right) at 15 and 250 mm depth, on the south wall for the period from June 2009June 2009 to June 2010

2.3 Material characterisation

The Castle of Chambord was mainly constructed in a soft-porous limestone, called tuffeau. This limestone dates from the Turonian age, the upper Cretaceous period, approximately 88-92 million years ago. Tuffeau was widely used in a number of castles in the Loire Valley because it is fine-grained, lightweight, shiny white in colour, and can be easily cut. It is characterized by a multi-scale pore size distribution, variable mineral composition and heterogeneous petrophysical properties (Beck et al., 2003). According to Folk's classification, tuffeau can be classified as a siliceous limestone that contains maritime fossils (coccoliths), reflecting its sedimentary origin. This highly porous limestone (porosity about 45%) is composed of 50% calcite and 30% silica in the form of opal cristobalite-tridymite, 10% quartz, and 10 % of clayey minerals (Dessandier, 2000), and is highly sensitive to moisture, Figure (3). Nowadays, tuffeau is still quarried in the area close to the Loire River.

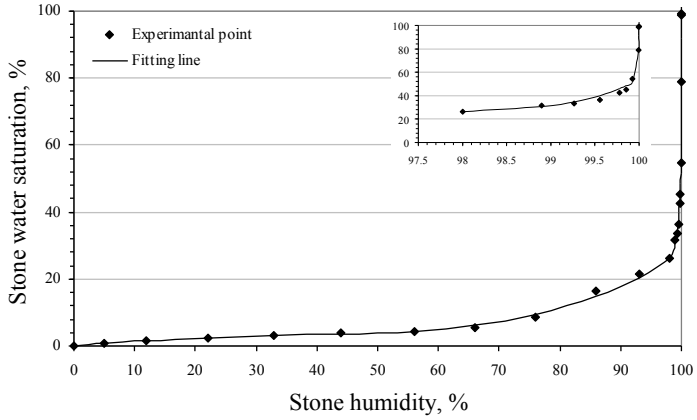

Figure 3: Relationship between stone humidity and degree of water saturation, (Beck, 2006)

The unconfined compressive strength (UCS) of tuffeau ranged between 12 MPa and 4.8 MPa for dry and fully saturated samples, respectively, while the indirect tensile strength values, measured by means of the Brazilian test, were 1.5 MPa for dry samples and 0.5 MPa for saturated samples (Beck, 2006). The relationships between the strength of tuffeau and water

saturation were fitted using logarithmic mathematical equations, as shown in Figure (4). These correlations are used later in this paper to estimate the strength of tuffeau at any water saturation.

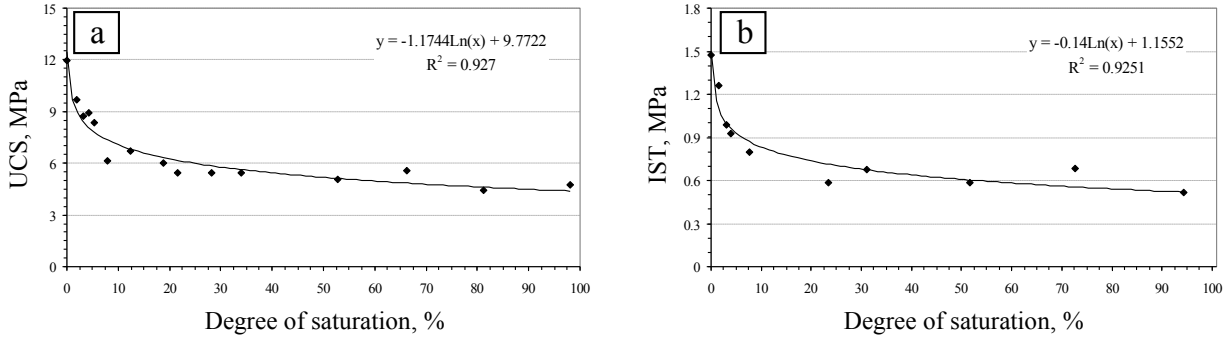

Figure 4: Correlation between degree of water saturation and Unconfined Compressive Strength, UCS (a), and Indirect Tensile strength, ITS (b), (Beck, 2006)

The elastic parameters (see section 2.4) used for calculation of the induced $\sigma_{T\text{-}H}$ can be obtained using Eqs.1, 2 and 3, at any stone temperature in the range from -8ºC to 40ºC and at any stone humidity between 0% and 100% (Al-Omari et al., 2014). These limits represent the extreme, but realistic, range of stone temperature and humidity measured in the field. The symbols (s and t) used in Eqs.3, 4 and 5 are the coded values obtained by the Design of Experiment (DOE) methodology used in this study. The coded values at different levels of stone temperature and stone water saturation (i.e. stone humidity) are listed in Table (1).

$$\varepsilon_{T\text{-}H} = [61.898 + 5.202t + 18.854s - 4.09t^2 + 1.519s^2 - 0.489ts - 3.944t^2s + 1.584ts^2 + 8.16t^3 + 0.565s^3 + 4.54t^3s + 0.965ts^3 + 5.53t^2s^2 - 2.36s^4 - 4.08t^3s^2 + 3.26t^2s^3 - 2.7t^3s^3] \cdot (10)^{-5} \quad \text{Eq.1}$$

$$E_{T\text{-}H} = 1570.775 + 17.303t + 19.098s + 6.02t^2 + 248.808s^2 - 94.496st + 11.67t^3 + 61.634st^2 - 92.936s^2t - 100.175s^3 - 19.486st^3 + 58.033s^3t + 191.29s^2t^2 - 127.7s^2t^3 + 80.14s^3t^2 + 21.89s^4t - 75.66s^3t^3 \quad \text{Eq.2}$$

$$\upsilon_{T-H} = 0.325 - 0.021t + 0.033s - 0.011st - 0.53s^2 + 0.021s^2t - 0.017st^2 + 0.016t^3 - 0.003s^3 + 0.012st^3 - 0.009s^2t^2 + 0.003s^3t + 0.008s^4 - 0.008s^2t^3 + 0.005s^3t^2 - 0.004s^4t - 0.005s^3t^3 + 0.004s^4t^2 \quad \text{Eq.3}$$

Table (1): Coding of the levels for stone temperature and stone water saturation (Al-Omari et al., 2014).

Variable	Temperature levels					Water saturation levels				
Value: T or S	-8ºC	2ºC	20ºC	40ºC		0%	7%	23%	80%	100%
Coding*: t or s	-1.442	-0.617	0.565	1.423		-1.930	-1.117	0.073	1.016	1.960
*Equation for temperature coding, $t = = -6.10^{-4}.T^2+0.0789.T-0.7726$										
*Equation for water saturation coding, $s = 1.28.10^{-5}.S^3-0.0022.S^2+0.1309.S-1.9298$										

2.4 Methods

The mathematical model (Eq.4) presented in previous studies (Bonazza et al., 2009a; Ponziani et al., 2012; Al-Omari et al., 2013a) was used to calculate the thermal stresses (σ_T) induced in the stone due to the daily variation in stone surface temperature. This equation refers to the mechanical response of a semi-infinite medium to restrained thermal dilation. The resulting

stress is calculated in the plane subjected to zero strain (i.e. the plane of the walls in the case of the Castle of Chambord). In the direction perpendicular to this plane, the strain is assumed to be free so the resulting stress is zero.

$$\sigma_T = \frac{E \cdot \alpha \cdot \Delta T}{1 - \upsilon} \qquad \text{Eq.4}$$

where:
E : The elastic modulus, Pa
α : The linear thermal expansion coefficient, $^{o}K^{-1}$
ΔT : The daily variation in stone surface temperature, °K
υ : The Poisson's ratio

In the present study the $\sigma_{T\text{-}H}$ generated inside the stones due to the variation in temperature and humidity were calculated by modifying Eq.4 to take the form below:

$$\sigma_{T-H} = \frac{E_{T-H} \cdot \varepsilon_{T-H}}{1 - \upsilon_{T-H}} \qquad \text{Eq.5}$$

Where the three elastic parameters - elastic modulus ($E_{T\text{-}H}$), Poisson's ratio ($\upsilon_{T\text{-}H}$) and strain ($\varepsilon_{T\text{-}H}$) - included in the modified model are functions of stone temperature and stone humidity. Since positive hygrothermal strain means positive dilation, the restriction of this positive strain generates compression. Consequently, when the result of Eq. 5 returned positive stresses, it corresponded to compression, while negative stresses meant tension.

The $\sigma_{T\text{-}H}$ stresses were calculated for each value of temperature and humidity collected (i.e. every 30 min during three years for each depth and wall orientation). The calculated $\sigma_{T\text{-}H}$ stresses were analyzed through two methods. The first one is called "daily variation in hygrothermal stresses". In this case the risk of damage induced to the stone due to the $\sigma_{T\text{-}H}$ was estimated with the methodology presented in previous work (Al-Omari et al., 2013a; Bonazza et al., 2009a; Ponziani et al., 2012). This method consisted in identifying the daily variation in stone stresses, i.e. the difference between the maximum and minimum stone stresses. This was done in an attempt to quantify the variations that may generate fatigue to the stones. These daily variations in stone stresses were divided by the lowest UCS calculated each day to represent the actual stress level as a proportion of the strength. In order to calculate the daily lowest UCS, the maximum stone humidity for each day was selected. Then Figure (3) was used to obtain the maximum stone saturation based on the maximum stone humidity. Finally, the minimum unconfined compressive stone strength was determined by using the formula presented in Figure (4-a).

The second method is called "maximum and minimum differential hygrothermal stresses". This new alternative consisted in computing the maximal and minimal stresses resulting from the daily variation in stone temperature and stone humidity, assuming a zero level of stress at 250 mm depth. These stresses were calculated by subtracting the stresses generated near the surface (at 15, 30 and 50 mm depth) from the stress measured at 250 mm depth. This depth is assumed to correspond to the mean state of the stone as it is very slightly affected by climatic variations (see Figure 2), allowing creep effects to stabilize.

In addition to these two methods, another parameter was studied: the correction of stone data. Since the accuracy of the sensors is not guaranteed in the 90-100% humidity range, the hypothesis that every value above 90% of humidity could be 99.99% (i.e. capillary saturation) was systematically tested. This hypothesis is supported by observations in the field: after heavy rainfall with significant wind, the humidity near the surface of stones is always randomly in the range 90-98 %, even if the surface is visually water saturated.

3. Results

3.1. Calculation of hygrothermal stresses

The results of both methods for stress calculation are presented in this section. For each result, two different hypotheses are presented: results based on actual stone data and results based on corrected stone data. Then, the damage risk assessment is presented for each method, and for each set of stone data.

3.1.1 Daily variation in hygrothermal stresses

The $\sigma_{T\text{-}H}$ calculated using Eq.5 was analyzed. Based on the original values of stone humidity, the daily variations in the $\sigma_{T\text{-}H}$ at three depths (15, 30 and 50 mm) inside the stones of both north and south walls, over a one-year period (June 2009June 2009 to June 2010), are presented in Figure (5). Figure (6) presents the same results when the calculations of the $\sigma_{T\text{-}H}$ were based on the adjusted stone humidity. The adjustment of the stones' humidity values resulted in an increase in the values of the daily variation in stone stresses, especially for the stone of the south walls.

3.1.2 Maximum and minimum differential hygrothermal stresses

Using the first method, it was possible to distinguish two extreme stresses (maximum and minimum) each day for each depth. By comparing these two extreme stresses and the reference stress at 250 mm depth the maximum and minimum differential stresses were calculated. When this differential stress was positive, it was compression, and tension when negative. The results of the analysis, based on the original stone humidity measurements, showed that, for both the north and south walls, the compression and tension stresses respectively reached 0.4 MPa and 0.3 MPa, Figure (7). The results in Figure (8) indicate that the adjustment of the stone humidity had little impact on the tensile stresses, while a clear effect was observed for the compressive stresses. The maximum/minimum stresses and the reference stress can both be positive as shown with the orange circles and both negative as shown with the black circles in Figure (7).

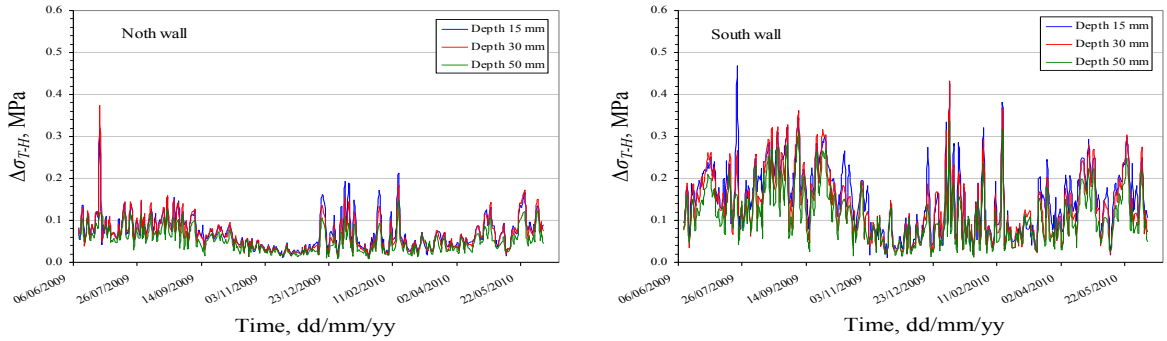

Figure 5: Daily variations in hygrothermal stresses at different depths inside the stone for the period from June 2009 to June 2010 on both, north wall (left), and south wall (right), based on the original stone humidity

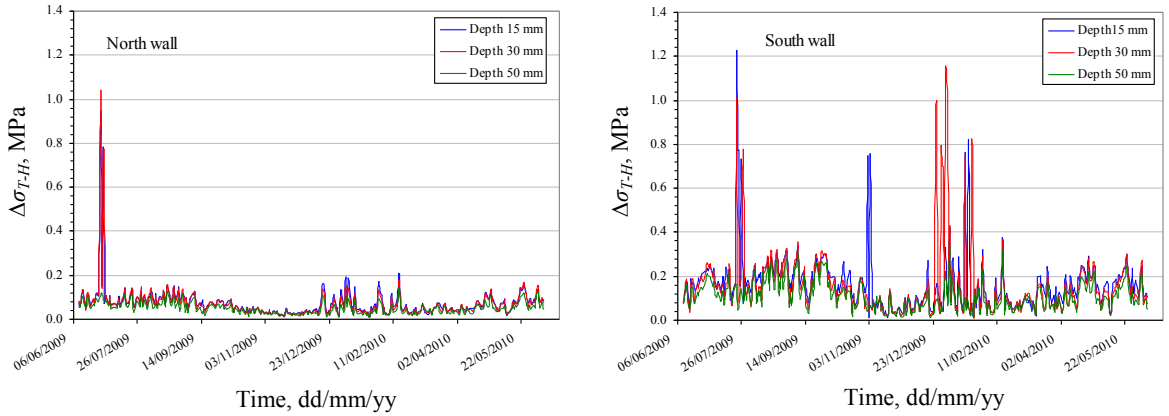

Figure 6: Daily variations in hygrothermal stresses at different depths inside the stone for the period from June 2009 to June 2010 on both, north wall (left), and south wall (right), based on the adjusted stone humidity

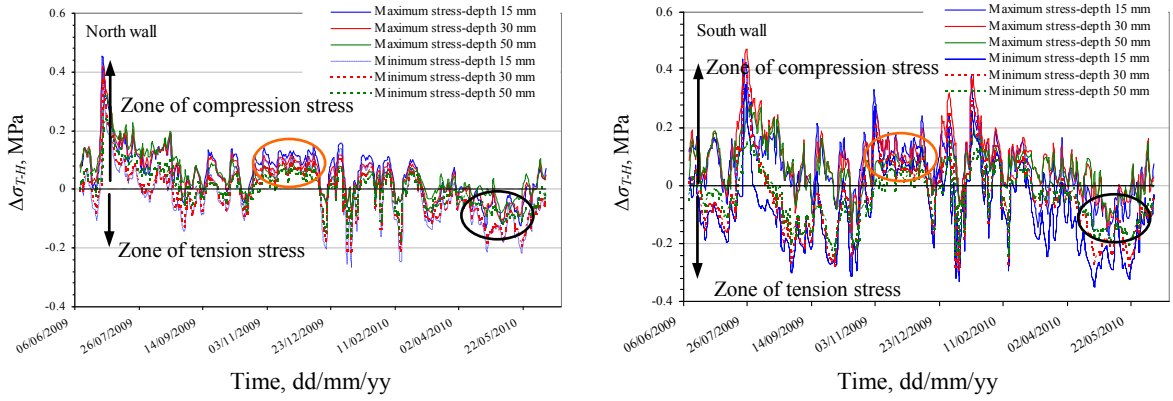

Figure 7: Maximum and minimum hygrothermal stresses at different depths inside the stone for the period from June 2009 to June 2010 on the north wall (left) and the south wall (right**),** based on the original stone humidity

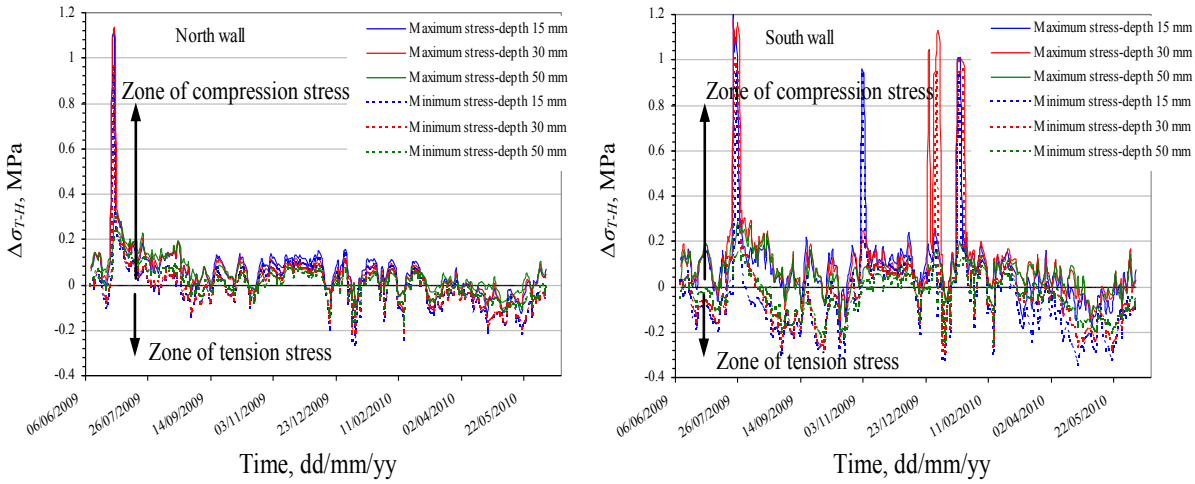

Figure 8: Maximum and minimum and tension hygrothermal stresses at different depths inside the stone for the period from June 2009 to June 2010 on the north wall (left) and the south wall (right), based on the adjusted stone humidity

3.2. Damage risk assessment

3.2.1. Damage due to daily variation in hydrothermal stresses

The σ_{T-H} stresses were compared with the minimum stone strength to assess the risk of damage to the stones located in the Castle of Chambord. In this case the daily variation in σ_{T-H}, for each day over the three-year period, was divided by the daily minimum stone strength. Figures (9 and 10) present an example of these daily variations during one year (from June 2009 to June 2010); the calculations were done by following the two bases adopted in the analysis, i.e. original and adjusted stone humidity.

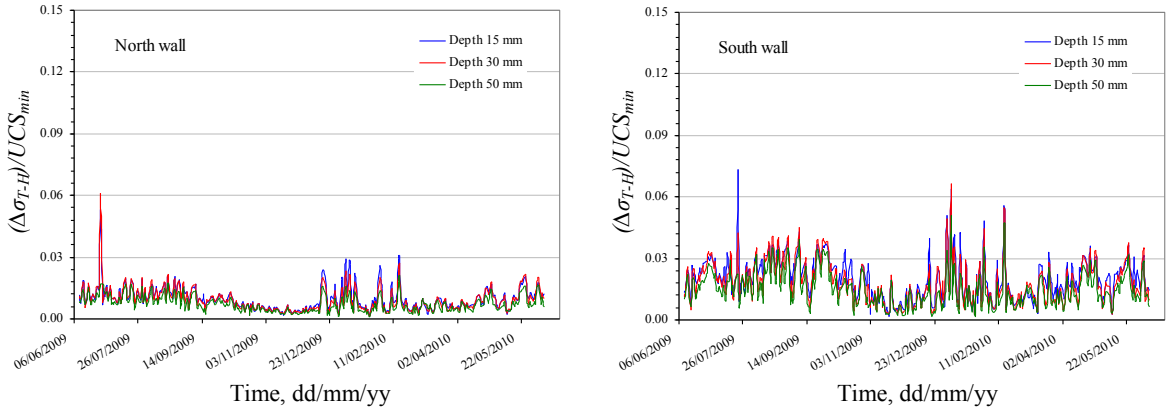

Figure 9: Proportion of daily variations in hygrothermal stresses to the minimum compression strength at different depths inside the stone for the period from June 2009 to June 2010 on both, north wall (left), and south wall (right), based on the original stone humidity

In this study, the damage to stone was estimated by comparing the σ_{T-H} with the maximum sustainable load. The maximum sustainable loads for the stone were obtained by dividing the unconfined compressive strength by a safety factor (Bonazza et al. 2009a; Ponziani et al., 2012; Al-Omari et al., 2013a). Table (2) lists the annual percentages of days with a daily variation of σ_{T-H} exceeding the maximum sustainable loads at different safety factors, over the three-year period for the north and south walls, and for the original set of humidity data. Table (3) presents the same results as those in Table (2) but the analysis is based on the adjusted stone humidity. The results show that, irrespective of the safety factor, the damage risk due to the daily variation in σ_{T-H} is several times higher for the analysis based on the adjusted stone humidity than for the analysis based on the original one.

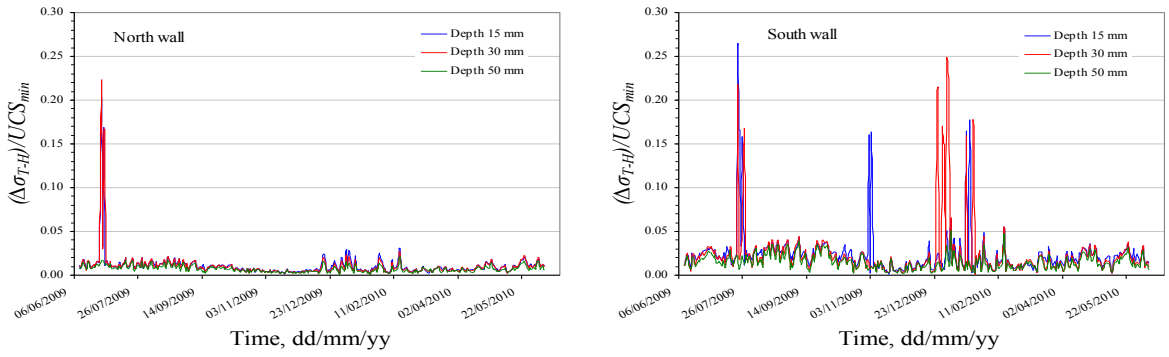

Figure 10: Proportion of daily variations in hygrothermal stresses to the minimum compression strength at different depths inside the stone for the period from June 2009 to

June 2010 on both, north wall (left), and south wall (right), based on the adjusted stone humidity

Table 2: Annual percentage of days with daily variation in hygrothermal stresses exceeding the sustainable load over the 3-year period (June 2009 to June/2012) for both north and south walls, depending on the safety factor, based on the original stone humidity

Safety factor	North				South		
	15 mm	30 mm	50 mm		15 mm	30 mm	50 mm
1	--	--	--		--	--	--
2	--	--	--		--	--	--
4	--	--	--		--	--	--
8	--	--	--		--	--	--
12	--	--	--		0.10	--	0.05
16	0.06	0.03	--		0.27	0.13	0.16
20	0.17	0.17	0.08		0.71	0.59	0.47

Table 4: Annual percentage of days with daily variation in hygrothermal stresses exceeding the sustainable load over the 3-year period (June 2009 to June/2012) for both north and south walls, depending on the safety factor, based on the adjusted stone humidity

Safety factor	North				South		
	15 mm	30 mm	50 mm		15 mm	30 mm	50 mm
1	--	--	--		--	--	--
2	--	--	--		--	--	--
4	--	--	--		0.02	--	--
8	0.88	1.14	0.12		1.51	1.79	--
12	0.94	1.20	0.15		1.63	1.93	0.05
16	1.02	1.27	0.16		1.70	2.09	0.16
20	1.14	1.39	0.25		2.09	2.40	0.47

3.2.2. Damage due to maximum and minimum differential hygrothermal stresses

The calculated compression and tension $\sigma_{T\text{-}H}$, based on the original stone humidity, were divided by the compressive and tensile strength, over the period from June 2009 to June 2010 for both the north and south walls, and are shown in Figure (11). Both the compressive and tensile strengths were obtained by using relationships presented in Figure (4) with the actual stone saturation values. Figure (12) presents the same approach with $\sigma_{T\text{-}H}$ based on the adjusted stone humidity. The damage to stone was estimated by comparing the $\sigma_{T\text{-}H}$ in compression and in tension with the compressive and tensile sustainable loads. The stone sustainable loads were obtained by dividing the compressive and tensile strength over a suitable safety factor. The analysis based on the original stone humidity, Table (4), lists the annual percentages of days with damage risk to the stone when compression and tension $\sigma_{T\text{-}H}$ exceed the sustainable loads both in compression and in tension conditions at different safety

factors over the period of three years for the north and the south walls. Table (5) presents the same results as Table (4) but the analysis is based on the adjusted stone humidity.

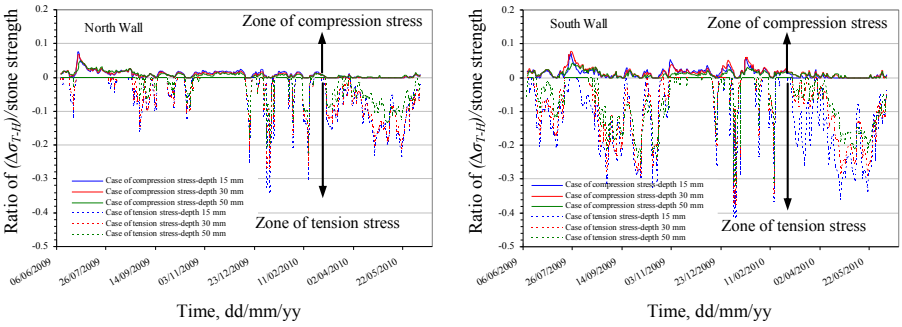

Figure 11: Proportion of compression, tension hygrothermal stresses to compressive, tensile stone strength at different depths inside the stone for the period from June 2009 to June 2010 on the north wall (left) and the south wall (right), based on the original stone humidity

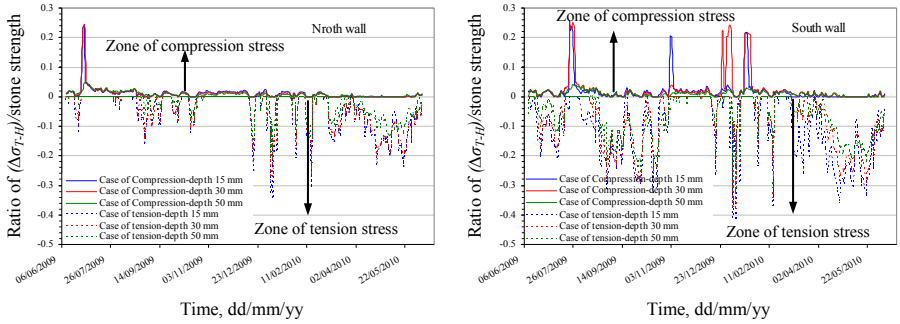

Figure 12: Proportion of compression, tension hygrothermal stresses to compressive, tensile stone strength at different depths inside the stone for the period from June 2009 to June 2010 on the north wall (left), and the south wall (right), based on the adjusted stone humidity.

Table 4: Annual percentage of the damage risk when the compression, tension hygrothermal stresses exceed the stone compressive, tensile strength over the 3-year period for both north and south walls, analysis based on the original stone humidity

Safety factor	Case of tension stress							Case of compression stress						
	North				South			North				South		
	15 mm	30 mm	50 mm		15 mm	30 mm	50 mm	15 mm	30 mm	50 mm		15 mm	30 mm	50 mm
1	--	--	--		--	--	--	--	--	--		--	--	--
2	0.70	0.64	0.61		--	0.08	0.23	--	--	--		--	--	--
4	3.89	2.98	2.09		16.77	8.53	2.18	--	--	--		--	--	--
8	26.29	18.93	5.68		54.61	42.97	30.90	--	--	--		--	--	--
12	42.82	38.16	19.67		68.40	60.06	46.92	--	--	--		0.35	0.02	--
16	54.99	51.59	34.33		76.25	69.92	58.88	0.29	0.29	--		0.80	1.03	--
20	63.39	60.65	45.28		82.11	75.82	66.17	0.74	0.54	--		1.67	3.14	--

Table 5: Annual percentage of the damage risk when the compression, tension hygrothermal stresses exceed the stone compressive, tensile strength over the 3-year period for both north and south walls, analysis based on the adjusted stone humidity

Safety factor	Case of tension stress							Case of compression stress						
	North				South			North				South		
	15 mm	30 mm	50 mm		15 mm	30 mm	50 mm	15 mm	30 mm	50 mm		15 mm	30 mm	50 mm
1	--	--	--		--	--	--	--	--	--		--	--	--
2	0.53	0.48	0.46		--	0.06	0.17	--	--	--		--	--	--
4	2.92	2.24	1.57		12.58	6.39	1.64	--	--	--		0.14	0.22	--
8	19.66	14.11	4.26		40.95	32.22	23.18	4.86	4.68	0.15		2.60	3.54	--
12	32.17	28.65	14.75		51.30	45.04	35.19	4.92	4.73	0.17		2.69	3.63	--
16	41.38	38.66	25.74		57.19	52.33	44.16	4.94	4.76	0.18		2.74	3.68	--
20	47.43	45.34	33.96		61.58	56.76	49.63	4.96	4.81	0.19		2.85	4.33	--

4. Discussion

The damage risk assessment performed in this study has thrown light on the effect of local factors such as the wall orientation or the depth inside the stone. These two local factors are discussed in this section. Moreover, as two different methods were used for stress calculation, in addition to the correction of stone data, these two methodological factors are also discussed.

4.1. Wall orientation

The fluctuations in the calculated $\sigma_{T\text{-}H}$ presented in Figures (5-12) were found to be higher in the stones in the South wall compared to the North wall. These findings can be attributed to the effect of direct insulation. The stones in the south wall are subjected to direct sun rays, leading to increased amplitude in the daily measurements of stone temperature and humidity. For example, the preliminary analysis of the stone data measured at the south wall showed that the daily variation in stone temperature and in stone humidity can exceed 20ºC and 30% respectively, while in the north wall these variations did not exceed 14ºC and 25%, respectively. The results presented in Tables 2 and 3 show that the stone orientation significantly affects the damage risk. The stones in the south wall are subjected to an increased damage risk compared with the stones in the north wall. This also holds for the compression and tension stresses calculated with the alternative methodology (Tables 4 and 5). This effect of wall orientation cannot be supported by in-situ observations since the dates of restoration are different for each span of the tower. However, this calculation tends to conclude that stones oriented southwards require finer monitoring and may require more frequent restoration compared to northward-facing stones.

4.2. Depth inside the stone

The results presented in Tables (2-5) show that, irrespective of the wall orientation, the methodology or the optional data correction, the damage risk decreases with depth. The decrease is significant from 15 mm to 30 mm and becomes even higher from 30 to 50 mm. As for wall orientation, this can be attributed to the lower amplitude of variation in temperature and humidity with depth. This is a consequence of the very fine porosity of tuffeau which results in a low thermal conductivity and low hygric diffusion coefficient. Of course, in-situ visual observations preferentially show surface damage, so no objective conclusion can be drawn from such observations. However, characterization of spalling revealed the presence of a crack network parallel to the surface, whose opening decreases with depth, suggesting that

damage decreases with depth (Janvier-Badosa et al., 2013). This observation supports the hypothesis that hygrothermal stresses could contribute to the damage process of spalling, as proposed by (Benavente et al., 2008; Colas et al., 2011).

4.3. Methodology of calculation

In this study, two methodologies were adopted in the analysis of the induced σ_{T-H}; by calculating σ_{T-H} as the difference between the daily maximum and minimum stresses (reference method), and by identifying the compression and tension stresses based on the comparison of the daily maximum and minimum stresses at depths up to 50 mm with the stone stresses at 250 mm depth (alternative method). Figures 5 and 6 show the σ_{T-H} obtained by the reference method. Because no stress sign can be extracted with the reference method, all the calculated stresses are assumed to be compression. The alternative method is able to differentiate compression stresses and tension stresses, as shown in Figure 7. The compression stresses calculated with the alternative method were found to be slightly higher than the compression stresses calculated by the reference method, especially for the stone in the north walls. As the tensile strength of tuffeau is much lower than its compressive strength, the calculation of tension stresses may be more critical. The data in Figure (7) showed that the tension stresses calculated with the alternative method reach 0.35 MPa, which corresponds to a non-nil damage risk with a safety factor of 2 and over. As for compression stresses, the risk is non-nil with a safety factor of 12 and over for the original set of stone data and 4 and over for the optional data correction, see Tables (4 and 5). Hence, the first damage is expected to occur for tension stresses, which would result in cracking of the stone/mortar interface. For high compression stresses, the main risk would be surface buckling. This type of instability could be a major factor for crack propagation or plate split-up when the cracks are parallel to the surface, especially if the thickness of the plate is low compared to its width, as for spalling (i.e. from 1 to 2 cm thick compared to 60 cm wide stones). Hence, tension damage would result in joint cracking while compression damage would result in spalling propagation or split-up. This mechanical analysis proves that it is relevant to calculate both tension and compression stresses, and so to promote the use of the alternative method.

4.4. Stone data correction

As the correction is only performed for days with relative humidity higher than 90%, and because it corresponds to days with heavy rain and wind, this data correction seems to be relevant. From the results presented in Figures (5 and 6) with the reference method, the effect of the stone data correction concerns only a few days in any given year. However, even in this situation, the damage risk is significantly higher for the results with the adjusted stone humidity (see Tables 2 and 3). The same is true of the results of the alternative method, but only for compression stresses. This is due to the fact that the data correction concerns only days with very high relative humidity that would result in positive hygric dilation if the strain were free and so compression since the strain is restrained. As a result, this correction only slightly affects the tension stress calculation, as can be seen in Figures (11 and 12) and Tables (4 and 5). The fact remains that stone data correction provides a significantly increased damage risk, from a minimal safety factor of 12 for compression stresses with the original set of data to only 4 for the same stresses with the adjusted stone humidity (see Table 5). This marked difference in the result demonstrates that sensor accuracy needs to be finer for high humidity so as to prevent any underestimation of the damage risk by compression.

5. Conclusion

This paper aimed to assess the risk of stone damage through the calculation of hygrothermal stresses, using a numerical model representing the effect of restrained dilation. To perform this analysis, it was necessary to first characterize the stone's hygrothermal elastic properties: elastic modulus, Poisson's ratio and hygrothermal strain. The climate data included in this calculation are the stone temperature and relative humidity, measured by sensors inserted into the stone at different depths. Particular attention must be paid when gathering core data; this was done here by inserting a sensor at 250 mm depth.

The reference method consisted in calculating the daily variation in hygrothermal stresses, and by dividing it by the minimal daily compressive strength of the stone. The damage risk was assessed by calculating the number of days with daily variation in stresses exceeding the maximum sustainable load, according to a given safety factor. The new alternative method proposed in this paper consisted in calculating the differential stresses between the surface sensors (15, 30 and 50 mm depth) and the core sensor (250 mm depth). This differential stress, either compression or tension, was divided by the compressive strength or the tensile strength, respectively. As for the reference method, the damage risk was assessed by calculating the number of days with tension or compression stresses exceeding the corresponding strength, according to a given safety factor.

The parameters studied were: the depth of sensors (15, 30, 50 and 250 mm); the wall orientation (North or South); the methodology (reference or alternative) and the optional stone data correction (original set or adjusted humidity). The study of this correction parameter was motivated by the fact that the accuracy of the sensors used at the Castle of Chambord is not guaranteed from 90 % to 100 % of relative humidity.

The results proved that the risk of damage to the stone can be significant. The first risk of damage is expected to occur in tension near the surface of the stone exposed to climate fluctuations. This would result in joint cracking. For higher safety factors, a significant risk of compression can occur. This would result in surface buckling, especially for stones already subjected to spalling, leading to crack propagation up to split-up. The damage risk decreases with depth and is higher on the south wall than on the north wall. The alternative methodology proved to be relevant for the calculation of both compression and tension stresses, which is useful to assess the consequences of the damage. The optional stone data correction proved to be relevant since the damage risk is significantly higher with this correction compared to the original set of data. This reveals that sensor accuracy is a significant issue for this calculation, and sensors with finer accuracy for high humidity should be preferred to avoid any underestimation of damage risk, especially in compression.

6. References

1. Al-Omari, A., Brunetaud, X., Beck, K., and Al-Mukhtar, M., (2013a), Effect of thermal stress, condensation and freezing–thawing action on the degradation of stones on the Castle of Chambord, France, Environmental earth science, DOI 10.1007/s12665-013-2782-4.

2. Al-Omari, A., Brunetaud, X., Beck, K., and Al-Mukhtar, M., (2013b), Experimental study on the role of freezing–thawing in the degradation of stones in the Castle of Chambord, Proceedings of International Conference on Built heritage, Milano, Italy.

3. Al-Omari, A., Brunetaud, X., Beck, K., and Al-Mukhtar, M., (2014), coupled thermal-hygric characterisation of elastic behaviour for soft and porous limestone, Construction and Building Materials, DOI: 10.1016/j.conbuildmat.2014.03.029.

4. Beck K. (2006), Etude des propriétés hydriques et des mécanismes d'altération de pierres calcaires à forte porosité. Ph.D. Thesis. University of Orleans, France.

5. Beck, K., Al-Mukhtar, M., Rozenbaum, O., and Rautureau, M., (2003), Characterisation, water transfer properties and deterioration in tuffeau: Building material in the Loire Valley, France, International Journal of Building and Environment, 38(9), pp 1151–1162.

6. Benavente, D., Cultrone, G., and Gomez-Heras M., (2008), The combined influence of mineralogical, hygric and thermal properties on the durability of porous building stones, European Journal of Mineralogy 20, pp 673–685.

7. Bonazza, A., Sabbioni, C., Messina, P., Guaraldi, C., and De Nuntiis, P., (2009a), Climate change impact: Mapping thermal stress on Carrara marble in Europe, Science of the Total Environment, 407, pp 4506–4512.

8. Bonazza, A., Messina, P., Sabbioni, C., Grossi, C.M., and Brimblecombe, P., (2009b), Mapping the impact of climate change on surface recession of carbonate buildings in Europe, Science of the Total Environment, 407, pp 2039–2050.

9. Camuffo, D., (1998), Microclimate for cultural heritage, Elsevier, Amsterdam.

10. Camuffo, D., and Sturaro, G., (2001), The climate of Rome and its action on monument decay, Climate Research, 6, pp 145–55.
11. Colas, E., Mertz, J.D., Thomachot-Schneider, C., Barbin, V., and Rassineux, F., (2011), Influence of the clay coating properties on the dilation behavior of sandstones, Applied Clay Science, 52(3), pp 245–252.

12. Dessandier, D., (2000), Guide méthodologique des monuments en termes de durabilité et compatibilité, in collaboration with Auger P., Haas H. and Hugues G. BRGM Report.

13. Eklund, S., (2008), Stone weathering in the monastic building complex on Mountain of St Aaron in Petra, Jordan, M.Sc. Thesis, University of Helsinki-Finland.

14. Janvier-Badosa, S., Beck, K., Brunetaud, X., and Al-Mukhtar, M., (2010), Characterization of stone weathering: a case study for Chambord castle, France, 8th International Symposium on the Conservation of Monuments in the Mediterranean Basin, Patras, Greece.

15. Janvier-Badosa, S., Beck, K., Brunetaud, X., and Al-Mukhtar, M., (2013), The occurrence of gypsum in the scaling of stones at the Castle of Chambord (France), Journal of Environmental Earth Sciences, DOI: 10.1007/s12665-013- 2865-2.

16. Moropoulou, A., Theoulakis, P., and Chrysophakis, T., (1995), Correlation between stone weathering and environmental factors in marine atmosphere, Atmospheric Environment, 29(8), pp 895–903.

17. Ponziani, D., Ferrero, E., Appolonia, L., and Migliorini, S., (2012), Effects of temperature and humidity excursions and wind exposure on the arch of Augustus in Aosta, Journal of Cultural Heritage, 13, pp 462–468.

18. Stefani, C., Brunetaud, X., Janvier-Badosa, S., Beck, K., De Luca, L., and Al-Mukhtar, M., (2013), Developing a toolkit for mapping and displaying stone alteration on a web-based documentation platform, Journal of Cultural Heritage, DOI: 10.1016/j.culher.2013.01.011.

19. Viles, H.A., (2005), Microclimate and weathering in the central Namib Desert, Namibia, Geomorphology 67, pp 189–209.